Proving the stability of the rolling navigation

Auguste Bourgois[1,2], Amine Chaabouni[3], Andreas Rauh[4] and Luc Jaulin[1]

[1] Ensta-Bretagne, Lab-STICC, Brest, France
[2] FORSSEA, Paris, France
[3] Ecole polytechnique, Palaiseau, France
[4]Carl von Ossietzky Universität Oldenburg, Germany

Abstract. In this paper, we propose to study the stability of a navigation method that allows a robot to move in an unstructured environment without compass by measuring a scalar function φ which only depends on the position. The principle is to ask the robot to *roll* along an isovalue of φ. Using an interval method, we prove the stability of our closed loop system in the special case where φ is linear.

1   Introduction

The rolling navigation has first been presented in [1] in the context of a small flying drone following the border of a cloud. The only exteroceptive information the robot has is if it is inside or outside the cloud. Experimentally, the control strategy has been proved to be very robust even if we do not know the prior shape of the cloud. The closed loop system corresponds to a nonlinear hybrid system and the theoretical analysis of the stability is considered as difficult.

The goal of this paper is to show that interval-based methods [2] can be used to provide a rigorous stability analysis of such a hybrid dynamical system. Interval analysis has indeed been used to solve numerous practical problems (see *e.g.*, [3] for solving nonlinear problems, [4, 5] for localization

and mapping, [6] for autonomous driving). In the context of dynamical systems and stability analysis, Tucker [7] has used interval analysis to prove that the Lorenz attractor exists and efficient solvers (such as CAPD) have been proposed for integrating differential equations [8][9] in a rigorous way. The corresponding methods can then be used for stability analysis of nonlinear systems [10, 11, 12]. In the context of hybrid systems, even if guaranteed integration has been used for characterizing reachability sets [13, 14], to our knowledge, it has never been used to check the stability of dynamical systems where jumps could occur.

The work is an extended version of the abstract presented for SCAN 2020 [15] which deals with the rigorous stability of hybrid systems. The main contribution of our paper is to propose a method which combines Poincaré maps with interval analysis in order to provide an attraction basin [16][17][18][19] associated with an hydrid system. More precisely, we want to find a subset of the state space which will converge to a stable periodic orbit.

Section 2 recalls the basic definitions related to Poincaré maps and stability analysis of nonlinear discrete-time systems. Section 3 formalizes the problem of the rolling-based navigation of robots in terms of hybrid systems. Section 4 proves the stability of the rolling-based navigation in the case where the environment is linear. Section 5 shows how the stability analysis can be used to compute a set of initial vectors which will converge to a stable attractor and Section 6 concludes the paper.

2 Mathematical tools

In this section, we give the basic tools that will be used to prove the stability of a periodic orbit of a hybrid system.

2.1 Discrete-time positive invariant set

Consider the discrete-time system

$$\mathbf{x}_{k+1} = \mathbf{f}(\mathbf{x}_k) \tag{1}$$

with $\mathbf{f}(\mathbf{0}) = \mathbf{0}$. A set $\mathbb{A}$ is positive invariant if $\mathbf{f}(\mathbb{A}) \subset \mathbb{A}$. We consider two types of sets for positive invariance: Ellipsoids or boxes.

Ellipsoid. Figure 1 (a) illustrates the case of a discrete-time system where the arrows represent the function $\mathbf{f}$. Subfigure (b) gives a positive invariant set.
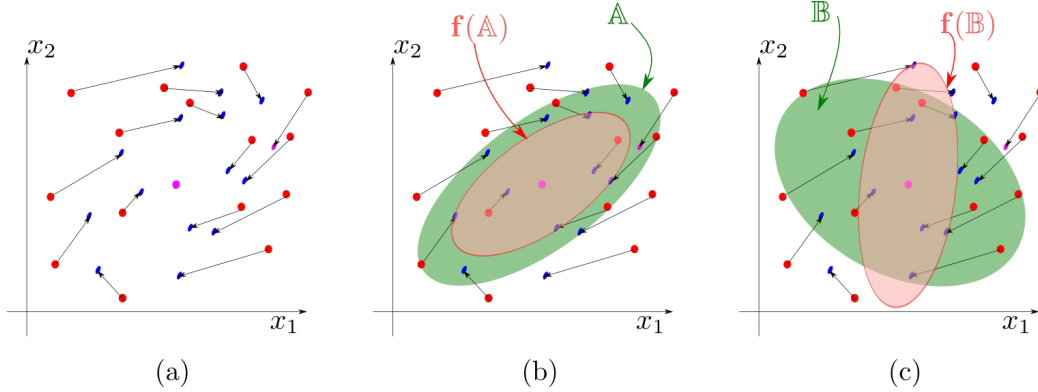
Figure 1: (a) A discrete-time system; (b) The green ellipse $\mathbb{A}$ is positive invariant; (c) The green ellipse $\mathbb{B}$ is not positive invariant

To find such an ellipsoid $\mathcal{E}_{\mathbf{x}} : \mathbf{x}^{\mathrm{T}} \cdot \mathbf{P} \cdot \mathbf{x} \leq \varepsilon$, we can use the Lyapunov method in the linear case. If the system is stable and linear, we have

$$\mathbf{x}_{k+1} = \mathbf{A} \cdot \mathbf{x}_k \tag{2}$$

and we can find a positive definite matrix $\mathbf{P}$ (denoted by $\mathbf{P} \succ 0$) such that $V(\mathbf{x}) = \mathbf{x}^{\mathrm{T}} \cdot \mathbf{P} \cdot \mathbf{x}$ is a Lyapunov function:

$$
\begin{aligned}
& V(\mathbf{x}_{k+1}) = V(\mathbf{x}_k) - \mathbf{x}_k^{\mathrm{T}} \mathbf{x}_k \\
\Leftrightarrow \quad & \mathbf{x}_{k+1}^{\mathrm{T}} \cdot \mathbf{P} \cdot \mathbf{x}_{k+1} = \mathbf{x}_k^{\mathrm{T}} \cdot \mathbf{P} \cdot \mathbf{x}_k - \mathbf{x}_k^{\mathrm{T}} \mathbf{x}_k \\
\Leftrightarrow \quad & \mathbf{x}_k^{\mathrm{T}} \cdot \mathbf{A}^{\mathrm{T}} \cdot \mathbf{P} \cdot \mathbf{A} \cdot \mathbf{x}_k - \mathbf{x}_k^{\mathrm{T}} \cdot \mathbf{P} \cdot \mathbf{x}_k = -\mathbf{x}_k^{\mathrm{T}} \mathbf{x}_k \\
\Leftrightarrow \quad & \mathbf{x}_k^{\mathrm{T}} \cdot \left(\mathbf{A}^{\mathrm{T}} \cdot \mathbf{P} \cdot \mathbf{A} - \mathbf{P}\right) \cdot \mathbf{x}_k = -\mathbf{x}_k^{\mathrm{T}} \mathbf{x}_k.
\end{aligned}
\tag{3}
$$

To determine the ellipsoid $\mathcal{E}_{\mathbf{x}}$, we have to solve the Lyapunov equation:

$$\mathbf{A}^{\mathrm{T}} \cdot \mathbf{P} \cdot \mathbf{A} - \mathbf{P} = -\mathbf{I} \tag{4}$$

which is linear in $\mathbf{P}$. If the system is nonlinear, we apply the Lyapunov method on the linearized system and check the positive invariance using interval analysis [10]. There, an ellipsoidal calculus method is presented that allows for finding domains that certainly belong to the region of attraction of a stable equilibrium. Due to the straightforward implementation of these approaches, they can serve as an initialization of advanced procedures for finding the maximal provable attraction domains of nonlinear systems for which advanced methods based on linear matrix inequality or Bezoutian approaches were developed in [20, 21]. For methods, optimizing the quadratic Lyapunov functions for a stability proof of nonlinear autonomous systems using interval analysis, see [22]. Combinations of these methods with the

box-type representation of invariant sets used in the remainder of this paper can be investigated in future work.

Boxes. To find a box which is positive invariant, we may use the centered form method [23, 10]. For this, check if

$$[\mathbf{J_f}]\,([\mathbf{x}]) \cdot [\mathbf{x}] \subset [\mathbf{x}] \tag{5}$$

where $\mathbf{J_f}(\mathbf{x})$ is the Jacobian matrix of $\mathbf{f}$ at $\mathbf{x}$ and $[\mathbf{J_f}]$ is its interval extension [2]. In some situations, such a box $[\mathbf{x}]$ does not exist. Now, for $k \in \{1, 2, \dots\}$, we have

$$\begin{aligned}
\mathbf{J_{f^k}} &= (\mathbf{J_f}(\mathbf{f}^{k-1})) \cdot \mathbf{J_{f^{k-1}}} \\
\mathbf{f}^k &= \mathbf{f} \circ \mathbf{f}^{k-1}.
\end{aligned} \tag{6}$$

In this case, we search for the smallest k such that

$$[\mathbf{J_{f^k}}]\,([\mathbf{x}]) \cdot [\mathbf{x}] \subset [\mathbf{x}], \tag{7}$$

where

$$\begin{aligned}
[\mathbf{J_{f^k}}]\,([\mathbf{x}]) &= [\mathbf{J_f}]([\mathbf{f}^{k-1}]([\mathbf{x}])) \cdot [\mathbf{J_{f^{k-1}}}]([\mathbf{x}]) \\
[\mathbf{f}^k]\,([\mathbf{x}]) &= [\mathbf{f}] \circ [\mathbf{f}^{k-1}]\,([\mathbf{x}])
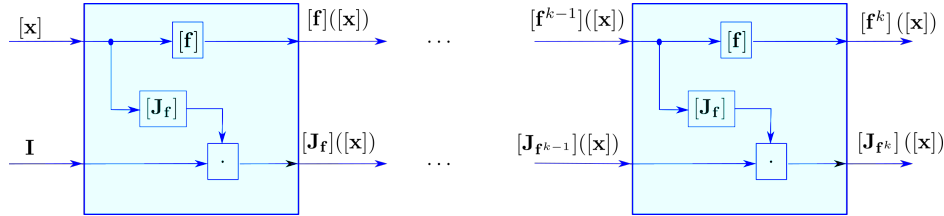\end{aligned} \tag{8}$$

as illustrated by Figure 2.

Figure 2: Sequential computation of $[\mathbf{f}^k]\,([\mathbf{x}])$ and $[\mathbf{J_{f^k}}]\,([\mathbf{x}])$

For instance, for $k = 2$, we have to check that

$$\underbrace{([\mathbf{J_f}]([\mathbf{f}]([\mathbf{x}]))) \cdot [\mathbf{J_f}]([\mathbf{x}]) \cdot [\mathbf{x}]}_{[\mathbf{J_{f^2}}]([\mathbf{x}])} \subset [\mathbf{x}]. \tag{9}$$

For both approaches, we need to have an interval extension for $\mathbf{f}$ and for its Jacobian matrix $\mathbf{J_f}$. It is not a problem when we have an analytical expression for $\mathbf{f}$ but this is not always the case as we will see in the following section.

2.2 Poincaré map

Consider now a continuous-time system of the form $\dot{\mathbf{x}} = \mathbf{f}(\mathbf{x})$, $\mathbf{x} \in \mathbb{R}^n$, such as the Van der Pol system illustrated by Figure 3 which contains a stable periodic orbit γ. To prove the stability of γ, we use the Poincaré method. For this, we choose a point $\mathbf{x}_0 \in \gamma$. Then, we chose a $n-1$ dimensional manifold $\mathcal{S}$ called the *Poincaré section*. The Poincaré section $\mathcal{S}$ is chosen transversal to the flow of the system. It is such that $\mathcal{S} \cap \gamma = \{\mathbf{x}_0\}$. We assume that the points of $\mathcal{S}$ all satisfy the equation $g(\mathbf{x}) = 0$.

Assume that we have a *Cartesian parametrization* for $\mathcal{S}$, *i.e.*, a diffeomorphism $\mathbf{h} : \mathcal{A} \mapsto \mathcal{S}$ such that $\mathbf{h}(\mathbf{0}) = \mathbf{x}_0$, where $\mathcal{A} = \mathbf{h}^{-1}(\mathcal{S}) \subset \mathbb{R}^{n-1}$. The function $\mathbf{h}$ is called the *chart* for $\mathcal{S}$. It allows us to fix a coordinate system on $\mathcal{S}$. Equivalently, when $\mathbf{a}$ scans $\mathcal{A}$, $\mathbf{h}(\mathbf{a})$ scans $\mathcal{S}$.
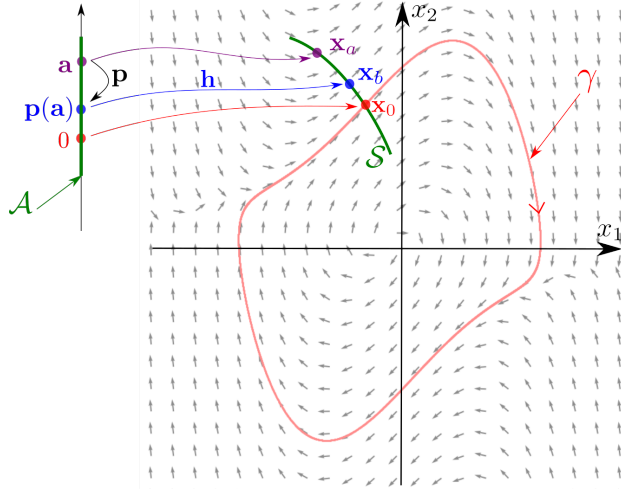

Figure 3: Stable periodic orbit (red) of a continuous time system

We define the Poincaré map by:

$$\mathbf{p} : \begin{array}{ccc} \mathcal{A} & \to & \mathcal{A} \\ \mathbf{a} & \mapsto & \mathbf{p}(\mathbf{a}) \end{array} \tag{10}$$

where $\mathbf{p}(\mathbf{a})$ is the point in $\mathcal{A} \subset \mathbb{R}^{n-1}$ such that the trajectory initialized at $\mathbf{x}_a = \mathbf{h}(\mathbf{a}) \in \mathbb{R}^n$ intersects $\mathcal{S}$ for the first time at $\mathbf{x}_b = \mathbf{h}(\mathbf{p}(\mathbf{a}))$. Then we define the discrete-time system

$$\mathbf{a}(k+1) = \mathbf{p}(\mathbf{a}(k)). \tag{11}$$

If the sequence is asymptotically stable, then γ is an attractor of the vector field $\mathbf{f}$. Equivalently, we will say that γ is stable.

Now, the asymptotic stability of the Poincaré map $\mathbf{p}$ can be proved using the Lyapunov method, as described in the previous section, combined with interval tools [24]. A three dimensional illustration of the Poincaré map is given in Figure 4. In the picture, both $\mathbf{a}$ and $\mathbf{p}(\mathbf{a})$ are represented in the 3D frame, at the places of $\mathbf{x}_a$ and $\mathbf{x}_b$, but they actually belong to the Cartesian plane $\mathbb{R}^2$ represented by the red base. For simplicity, we may confuse the part of the hyperplane $\mathcal{A} \subset \mathbb{R}^{n-1}$ and the surface $\mathcal{S}$.

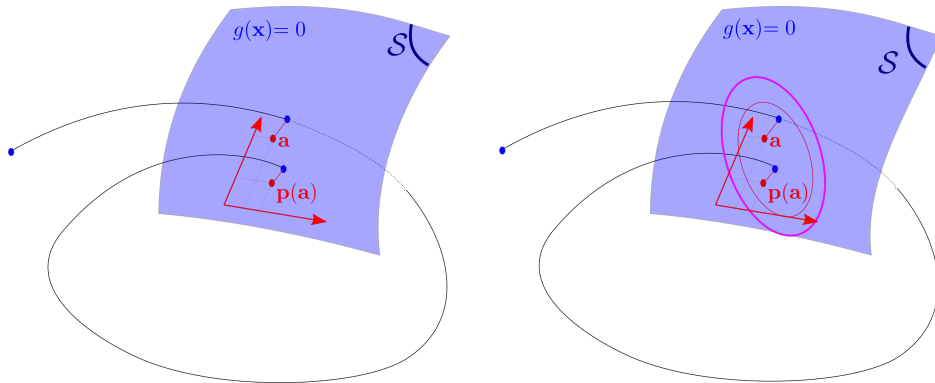

Figure 4: Poincaré map (left); Positive invariant ellipsoid of the Poincaré section (right)

2.3 Partial Poincaré maps

Hybrid systems [25], is a class of dynamical systems with discrete state q (for instance $q \in \{0, 1\}$) and a continuous state $\mathbf{x} \in \mathbb{R}^n$. The continuous state $\mathbf{x}$ follows a state equation of the form

$$\dot{\mathbf{x}} = \mathbf{f}(\mathbf{x}, q).$$

When some equality conditions are satisfied for $\mathbf{x}$, say $g(\mathbf{x}, q) = 0$ then q may jump from one discrete state to another (*e.g.*, from $q = 0$ to $q = 1$). The state vector $\mathbf{x}$ may jump also. For hybrid systems, we need more than one section to prove the stability [26]. An illustrative example will be given in Section 4. Since we have several sections, we will have several Poincaré maps. They will be called *partial* Poincaré maps. These maps also exist for dynamical systems that are not hybrid, but they are not strictly needed.

Figure 5 represents a situation with two sections $\mathcal{S}_1$, $\mathcal{S}_2$ and the partial Poincaré map is $\mathbf{p} : \mathcal{S}_1 \mapsto \mathcal{S}_2$ which is defined from a state equation of the form $\dot{\mathbf{x}} = \mathbf{f}(\mathbf{x})$. We assume that it is possible to get a Cartesian frame for $\mathcal{S}_1$ and $\mathcal{S}_2$ thanks to charts $\mathbf{h}_1$ and $\mathbf{h}_2$. Using these charts we can define boxes on these sections.
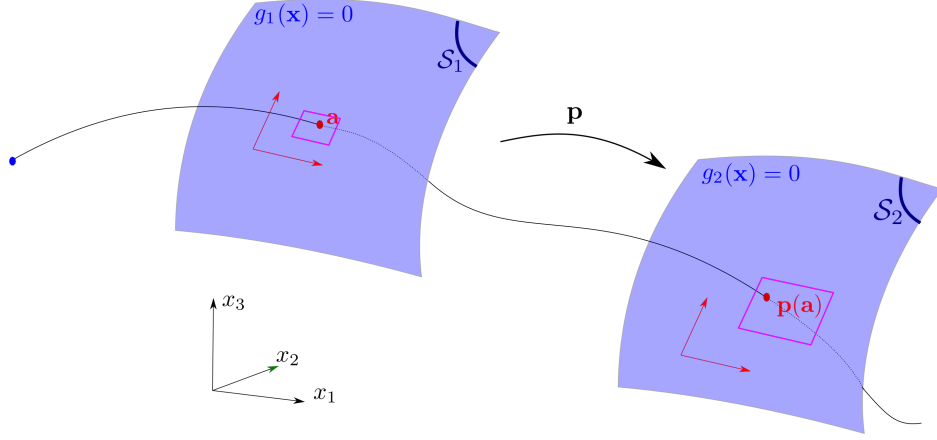
Figure 5: Partial Poincaré map to go from one section to another

2.4 Interval extension for the Poincaré map

Consider the system

$$\dot{\mathbf{x}} = \mathbf{f}(\mathbf{x}) \tag{12}$$

where $\mathbf{f} : \mathbb{R}^n \mapsto \mathbb{R}^n$ is C^1 and Lipschitz continuous. The flow of the system is denoted by $\mathbf{\Phi}(\mathbf{x}_0, t)$. Take two Poincaré sections $\mathcal{S}_1, \mathcal{S}_2$ with charts $\mathbf{h}_1, \mathbf{h}_2$. We assume that $\mathcal{S}_1 \cap \mathcal{S}_2 = \emptyset$ and any trajectory initialized in $\mathcal{S}_1$, will cross $\mathcal{S}_2$ later. Define the two sets $\mathcal{A}_1 = \mathbf{h}_1^{-1}(\mathcal{S}_1) \subset \mathbb{R}^{n-1}$ and $\mathcal{A}_2 = \mathbf{h}_2^{-1}(\mathcal{S}_2) \subset \mathbb{R}^{n-1}$. Take a point $\mathbf{a} \in \mathcal{A}_1$ and denote by $\mathbf{x}_a = \mathbf{h}_1(\mathbf{a})$ the corresponding state vector in $\mathcal{S}_1 \subset \mathbb{R}^n$. The trajectory initialized at $\mathbf{x}_a$ will cross $\mathcal{S}_2$ for the first time at $\mathbf{x}_b \in \mathbb{R}^n$ at time τ_b. Define by $\mathbf{b} = \mathbf{h}_2^{-1}(\mathbf{x}_b) \in \mathcal{A}_2$. Note that $\mathbf{a}$ and $\mathbf{x}_a$ correspond to the same quantity except that $\mathbf{a} \in \mathcal{A}_1$ whereas $\mathbf{x}_a \in \mathcal{S}_1 \subset \mathbb{R}^n$. The same remark could be done for the pair $(\mathbf{b}, \mathbf{x}_b)$. The Poincaré map $\mathbf{b} = \mathbf{p}(\mathbf{a})$ is here defined as the following composition:

$$\mathbf{a} \in \mathcal{A}_1 \subset \mathbb{R}^{n-1} \mapsto \mathbf{x}_a \in \mathcal{S}_1 \subset \mathbb{R}^n \mapsto \mathbf{x}_b = \mathbf{\Phi}(\mathbf{x}_a, \tau_b) \in \mathcal{S}_2 \subset \mathbb{R}^n \mapsto \mathbf{b} \in \mathcal{A}_2 \subset \mathbb{R}^{n-1}.$$

We want an interval extension for $\mathbf{p}$. We propose the following algorithm with the illustrating Figure 6.

Step 1. Take a box $[\mathbf{a}] \subset \mathcal{A}_1 \subset \mathbb{R}^{n-1}$ and compute $[\mathbf{x}_a] = [\mathbf{h}_1]([\mathbf{a}])$, where $[\mathbf{h}_1]$ is the interval extension of the chart $\mathbf{h}_1$.

Step 2. Integrate $[\mathbf{x}_a]$ to get a tube $[\mathbf{x}](\cdot)$ of $\mathbb{R}^n$. Note that $[\mathbf{x}](0) = [\mathbf{x}_a]$

Step 3. We compute the tubes $[y](\cdot) = [g_2]([\mathbf{x}](\cdot))$ and the tube $[\dot{y}](\cdot) = [\frac{\partial g_2}{\partial \mathbf{x}}] \cdot [\mathbf{f}]([\mathbf{x}](\cdot))$ and we select an interval $[t_1, t_2]$ which satisfies

$$
\begin{array}{lll}
(i) & [y]([0, t_1]) \subset]0, \infty] & \\
(ii) & [y]([t_2]) \subset [-\infty, 0[& \tag{13} \\
(iii) & [\dot{y}]([t_1, t_2])) \subset [-\infty, 0[&
\end{array}
$$

If we fail to find this interval, we return a failure.

Step 4. Select the subtube $[\mathbf{x}]([t_1, t_2])$.

Step 5. Return a box $[\mathbf{x}_b] \subset \mathbb{R}^n$ which encloses the subtube $\cup_{t \in [t_1, t_2]}[\mathbf{x}](t)$.

Step 6. Compute a box $[\mathbf{b}]$ which encloses $\mathbf{h}_2^{-1}([\mathbf{x}_b] \cap \mathcal{S}_2)$
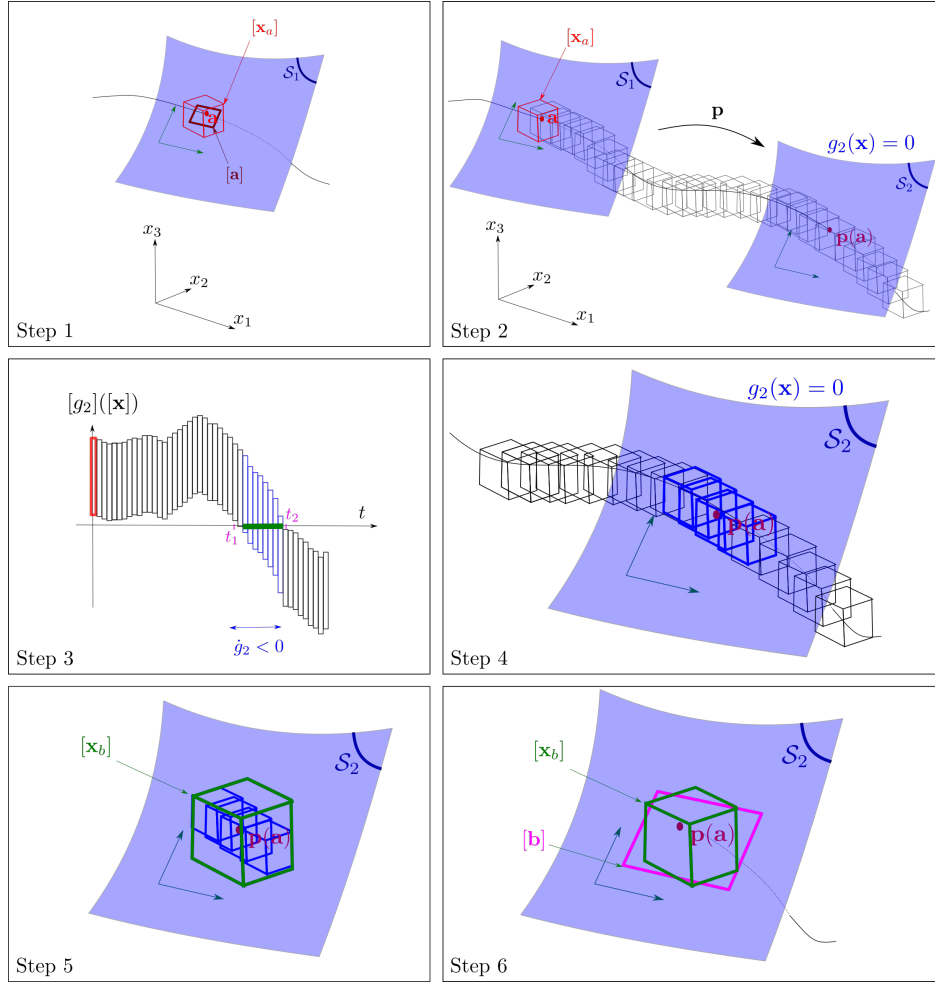

Figure 6: Poincaré interval extension

2.5 Variational equation

Consider again the system

$$\dot{\mathbf{x}} = \mathbf{f}(\mathbf{x}), \ \mathbf{x} \in \mathbb{R}^n \tag{14}$$

where $\mathbf{f}$ is now assumed to be twice differentiable. Denote by $\mathbf{\Phi}(\mathbf{x}_0, t)$ the flow for an initial vector $\mathbf{x}_0$. We define the *variational matrix* $\mathbf{J}(\mathbf{x}_0, t) = \frac{\partial \mathbf{\Phi}(\mathbf{x}_0, t)}{\partial \mathbf{x}_0}$.

It describes the effect of a small perturbation on a given trajectory, while we make a small variation on the initial state vector $\mathbf{x}_0$. It can be shown that it satisfies the *variational equation [27]*

$$\dot{\mathbf{J}} = \frac{\partial \mathbf{f}(\mathbf{x})}{\partial \mathbf{x}} \cdot \mathbf{J}, \tag{15}$$

with $\mathbf{J}(0) = \mathbf{I}$ for which further applications are discussed with respect to sensitivity analysis and control design in [28]. Using an interval ODE solver, we get an enclosure for $\mathbf{x}(t)$ and $\mathbf{J}(t)$, for a given initial box $[\mathbf{x}_0]$.

2.6   Jacobian of the Poincaré map

Proposition 1. *Consider a state equation with a flow $\mathbf{\Phi}(\mathbf{x}, t)$ and two Poincaré sections $\mathcal{S}_1$, $\mathcal{S}_2$ with equations $g_1(\mathbf{x}) = 0$, $g_2(\mathbf{x}) = 0$. The associated charts for $\mathcal{S}_1$ and $\mathcal{S}_2$ are denoted by $\mathbf{h}_1, \mathbf{h}_2$. Define $\mathcal{A}_1 = \mathbf{h}_1^{-1}(\mathcal{S}_1)$ and $\mathcal{A}_2 = \mathbf{h}_2^{-1}(\mathcal{S}_2)$. Denote by $\mathbf{p} : \mathcal{A}_1 \to \mathcal{A}_2$ the associated partial Poincaré map and by*

$$\tau(\mathbf{x}) = \min\{t > 0 | \mathbf{\Phi}(\mathbf{x}, t) \in \mathcal{S}_2\} \tag{16}$$

the associated Poincaré time function, which is assumed to exist for all $\mathbf{x} \in \mathcal{A}_1$. Take $\mathbf{a} \in \mathcal{A}_1$. We have

$$\mathbf{J}_\mathbf{p}(\mathbf{a}) = \frac{\partial \mathbf{p}}{\partial \mathbf{a}}(\mathbf{a}) = \frac{\partial \mathbf{h}_2^{-1}}{\partial \mathbf{x}}(\mathbf{x}_b) \cdot \frac{\partial \mathbf{q}}{\partial \mathbf{x}}(\mathbf{x}_a) \cdot \frac{\partial \mathbf{h}_1}{\partial \mathbf{a}}(\mathbf{a}), \tag{17}$$

where

$$\begin{array}{llll} (i) & \mathbf{q}(\mathbf{x}_a) & = & \mathbf{\Phi}(\mathbf{x}_a, \tau(\mathbf{x}_a)) \\ (ii) & \frac{\partial \mathbf{q}}{\partial \mathbf{x}}(\mathbf{x}_a) & = & \mathbf{J}_m + \mathbf{f}(\mathbf{x}_b) \cdot \frac{\partial \tau}{\partial \mathbf{x}}(\mathbf{x}_a) \\ (iii) & \frac{\partial \tau}{\partial \mathbf{x}}(\mathbf{x}_a) & = & -\frac{1}{\frac{\partial g_2}{\partial \mathbf{x}}(\mathbf{x}_b) \cdot \mathbf{f}(\mathbf{x}_b)} \cdot \frac{\partial g_2}{\partial \mathbf{x}}(\mathbf{x}_b) \cdot \mathbf{J}_m \end{array} \tag{18}$$

and

$$\begin{array}{lll} \mathbf{x}_a & = & \mathbf{h}_1(\mathbf{a}), \mathbf{a} \in \mathbb{R}^{n-1} \\ \mathbf{x}_b & = & \mathbf{h}_2(\mathbf{b}), \mathbf{b} \in \mathbb{R}^{n-1} \\ \mathbf{b} & = & \mathbf{p}(\mathbf{a}) \\ \mathbf{J}_m & = & \frac{\partial \mathbf{\Phi}}{\partial \mathbf{x}}(\mathbf{x}_a, \tau(\mathbf{x}_a)) \qquad \textit{(monodromy matrix)}. \end{array} \tag{19}$$

In this expression, $\frac{\partial \mathbf{h}_2^{-1}}{\partial \mathbf{x}}(\mathbf{x}_b)$, is the generalized inverse, i.e.

$$\frac{\partial \mathbf{h}_2^{-1}}{\partial \mathbf{x}}(\mathbf{x}_b) = \left(\left(\frac{\partial \mathbf{h}_2}{\partial \mathbf{x}}(\mathbf{b}) \right)^T \left(\frac{\partial \mathbf{h}_2}{\partial \mathbf{x}}(\mathbf{b}) \right) \right)^{-1} \left(\frac{\partial \mathbf{h}_2}{\partial \mathbf{x}}(\mathbf{b}) \right)^T. \tag{20}$$

Proof. The computation will be based on the composition of Figure 7.   □
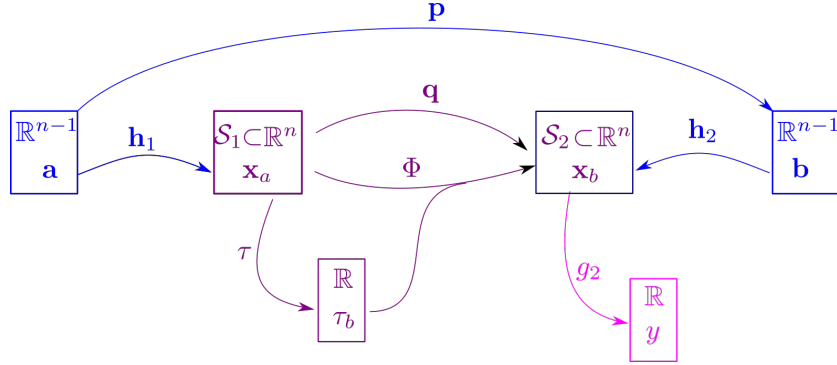
Figure 7: Composition of functions used to compute the Jacobian of the Poincaré map

Define

$$
\begin{aligned}
y &= g_2(\mathbf{x}_b) \\
\mathbf{x}_b &= \mathbf{\Phi}(\mathbf{x}_a, \tau_b) \\
\tau_b &= \tau(\mathbf{x}_a).
\end{aligned}
\tag{21}
$$

We have

$$
\begin{aligned}
dy &= \frac{\partial g_2}{\partial \mathbf{x}}(\mathbf{x}_b) \cdot d\mathbf{x}_b \\
d\mathbf{x}_b &= \frac{\partial \mathbf{\Phi}}{\partial \mathbf{x}}(\mathbf{x}_a, \tau_b) \cdot d\mathbf{x}_a + \underbrace{\frac{\partial \mathbf{\Phi}}{\partial t}(\mathbf{x}_a, \tau_b)}_{\mathbf{f}(\mathbf{x}_b)} \cdot d\tau_b \\
d\tau_b &= \frac{\partial \tau}{\partial \mathbf{x}}(\mathbf{x}_a) \cdot d\mathbf{x}_a.
\end{aligned}
\tag{22}
$$

Thus

$$
\begin{aligned}
dy &= \frac{\partial g_2}{\partial \mathbf{x}}(\mathbf{x}_b) \cdot d\mathbf{x}_b \\
&= \frac{\partial g_2}{\partial \mathbf{x}}(\mathbf{x}_b) \cdot \left(\frac{\partial \mathbf{\Phi}}{\partial \mathbf{x}}(\mathbf{x}_a, \tau_b) \cdot d\mathbf{x}_a + \mathbf{f}(\mathbf{x}_b) \cdot d\tau_b \right) \\
&= \frac{\partial g_2}{\partial \mathbf{x}}(\mathbf{x}_b) \cdot \left(\frac{\partial \mathbf{\Phi}}{\partial \mathbf{x}}(\mathbf{x}_a, \tau_b) \cdot d\mathbf{x}_a + \mathbf{f}(\mathbf{x}_b) \cdot \frac{\partial \tau}{\partial \mathbf{x}}(\mathbf{x}_a) \cdot d\mathbf{x}_a \right).
\end{aligned}
\tag{23}
$$

Since $dy = 0$, we get

$$
\frac{\partial g_2}{\partial \mathbf{x}}(\mathbf{x}_b) \cdot \mathbf{f}(\mathbf{x}_b) \cdot \frac{\partial \tau}{\partial \mathbf{x}}(\mathbf{x}_a) = -\frac{\partial g_2}{\partial \mathbf{x}}(\mathbf{x}_b) \cdot \frac{\partial \mathbf{\Phi}}{\partial \mathbf{x}}(\mathbf{x}_a, \tau_b),
\tag{24}
$$

i.e.

$$
\frac{\partial \tau}{\partial \mathbf{x}}(\mathbf{x}_a) = -\frac{1}{\frac{\partial g_2}{\partial \mathbf{x}}(\mathbf{x}_b) \cdot \mathbf{f}(\mathbf{x}_b)} \cdot \frac{\partial g_2}{\partial \mathbf{x}}(\mathbf{x}_b) \cdot \frac{\partial \mathbf{\Phi}}{\partial \mathbf{x}}(\mathbf{x}_a, \tau_b),
\tag{25}
$$

which corresponds to (iii).

As a consequence

$$
\begin{aligned}
d\mathbf{x}_b &= \frac{\partial \mathbf{\Phi}}{\partial \mathbf{x}}(\mathbf{x}_a, \tau_b) \cdot d\mathbf{x}_a + \mathbf{f}(\mathbf{x}_b) \cdot d\tau_b \\
&= \frac{\partial \mathbf{\Phi}}{\partial \mathbf{x}}(\mathbf{x}_a, \tau_b) \cdot d\mathbf{x}_a + \mathbf{f}(\mathbf{x}_b) \cdot \frac{\partial \tau}{\partial \mathbf{x}}(\mathbf{x}_a) \cdot d\mathbf{x}_a,
\end{aligned}
\tag{26}
$$

i.e.,

$$\frac{\partial \mathbf{q}}{\partial \mathbf{x}}(\mathbf{x}_a) = \frac{\partial \mathbf{\Phi}}{\partial \mathbf{x}}(\mathbf{x}_a, \tau(\mathbf{x}_a)) + \mathbf{f}(\mathbf{x}_b) \cdot \frac{\partial \tau}{\partial \mathbf{x}}(\mathbf{x}_a), \tag{27}$$

which corresponds to (ii).

The expression for $\mathbf{J_p}(\mathbf{a})$ is directly obtained from the chain rule. ∎

Remark 2. The function $\mathbf{h}_2 : \mathcal{A}_2 \mapsto \mathcal{S}$ is a diffeomorphism and we have an expression for it. For instance, it could be

$$\mathbf{h}_2(a_1, a_2) = \begin{pmatrix} a_1 + a_2 \\ a_1 - a_2 \\ a_1 \end{pmatrix} \tag{28}$$

if we choose $\mathbf{h}_2$ linear. We have $\mathbf{h}_2(\mathbb{R}^2) = \mathcal{S}_2$ which is a two-dimensional plane of $\mathbb{R}^3$. To apply the chain rule, we need the Jacobian matrix for $\mathbf{h}_2^{-1}$. Several expressions exist for it. One of them is the generalized inverse given here by

$$\mathbf{h}_2^{-1} = \begin{pmatrix} \frac{1}{3}(x_1 + x_2 + x_3) \\ \frac{1}{2}(x_1 - x_2) \end{pmatrix}. \tag{29}$$

Indeed

$$\mathbf{h}_2^{-1} \circ \mathbf{h}_2(a_1, a_2) = \begin{pmatrix} \frac{1}{3}(a_1 + a_2 + a_1 - a_2 + a_1) \\ \frac{1}{2}(a_1 + a_2 - (a_1 - a_2)) \end{pmatrix} = \begin{pmatrix} a_1 \\ a_2 \end{pmatrix}. \tag{30}$$

Since we have chosen $\mathbf{h}_2$ linear, the function and its Jacobian are similar. The goal of this remark is to explain why we need the generalized inverse (20) whereas $\mathbf{h}_2$ is a diffeomorphism: it is due to the fact that $\mathbf{h}_2$ needs to be represented as a function from $\mathbb{R}^{n-1}$ to $\mathbb{R}^n$.

2.7   Interval extension of its Jacobian

To get an interval extension of the Jacobian matrix $\mathbf{J_p}$ of the Poincaré map, we integrate the variational equation using an interval integration scheme such as the Lohner method [29]. We get a tube $[\mathbf{J}](t)$ and we select the smallest interval matrix which encloses the *monodromy matrix* $[\mathbf{J}]([\tau_b])$, where $[\tau_b]$ is the time interval computed in Section 2.4. The following algorithm computes the Jacobian matrix $\mathbf{J_p}$ for $\mathbf{p}$. Note that this algorithm is not new and can be seen as a simplified version of existing algorithms, see *e.g.,* [8] [30] [31].

Algorithm. INTERVALPOINCARÉJACOBIAN. In: $\mathbf{f}, [\mathbf{a}]$ Out:$[\mathbf{J_p}]$

1. $[\mathbf{x}_a] = [\mathbf{h}_1]([\mathbf{a}])$
2. Compute the tubes $[\mathbf{x}](t) = [\mathbf{\Phi}]([\mathbf{x}_a], t)$ and $[\mathbf{J}](t) = [\frac{\partial \mathbf{\Phi}}{\partial \mathbf{x}}]([\mathbf{x}_a], t)$
3. From $g_2([\mathbf{x}](t))$, select the Poincaré time interval $[\tau_b]$ (see Section 2.4)
4. $[\mathbf{x}_b] = [\mathbf{x}]([\tau_b])$
5. $[\mathbf{J}_m] = [\mathbf{J}]([\tau_b])$ (monodromy matrix)
6. $[\mathbf{J}_q] = \left(\mathbf{I} - \frac{[\mathbf{f}]([\mathbf{x}_b]) \cdot \left(([\frac{\partial g_2}{\partial \mathbf{x}}]([\mathbf{x}_b])) \right)}{[\mathbf{J}_{g_2}] \cdot [\mathbf{f}]([\mathbf{x}_b])} \right) \cdot [\mathbf{J}_m]$
7. $[\mathbf{b}] = [\mathbf{h}_2^{-1}]([\mathbf{x}_b])$
8. $[\mathbf{H}_2] = [\frac{\partial \mathbf{h}_2}{\partial \mathbf{b}}]([\mathbf{b}])$
9. $[\mathbf{J_p}] = \left(([\mathbf{H}_2^{\mathrm{T}}] \cdot [\mathbf{H}_2])^{-1} [\mathbf{H}_2^{\mathrm{T}}] \right) \cdot [\mathbf{J}_q] \cdot [\frac{\partial \mathbf{h}_1}{\partial \mathbf{a}}]([\mathbf{a}])$

2.8   Example

We choose a very simple example to illustrate the principle of the procedure INTERVALPOINCARÉJACOBIAN. We have chosen this example for the following reasons:

- It is related to the application that will be considered in Section 3

- It can be executed analytically by hand by the reader for a better understanding of the approach.

- The example will allow us to produce a 3D figure which illustrates clearly the principle of our method.

Consider the system

$$\begin{cases} \dot{x}_1 &= \quad 1 \\ \dot{x}_2 &= \quad \sin x_3 \\ \dot{x}_3 &= \quad 1. \end{cases} \tag{31}$$

We assume that we have two surfaces

$$\begin{aligned} \mathcal{S}_1 &= \{\mathbf{x} \,|\, x_1 = 0\} \\ \mathcal{S}_2 &= \{\mathbf{x} \,|\, x_2 = 0\}. \end{aligned} \tag{32}$$

We fix the coordinate frames of these surfaces by choosing the origins $\mathbf{o}_1 = (0, 0, \frac{\pi}{2})$, $\mathbf{o}_2 = (\pi, 0, \frac{3\pi}{2})$ and the basis $\mathbf{i}_1 = (0, 1, 0)$, $\mathbf{j}_1 = (0, 0, 1)$ for $\mathcal{S}_1$. The basis for $\mathcal{S}_2$ is chosen as $\mathbf{i}_2 = (1, 0, 0)$, $\mathbf{j}_2 = (0, 0, 1)$. Thus, the charts are

$$\mathbf{h}_1(\mathbf{a}) = \begin{pmatrix} 0 \\ a_1 \\ a_2 \end{pmatrix} + \mathbf{o}_1 = \begin{pmatrix} 0 \\ a_1 \\ a_2 + \frac{\pi}{2} \end{pmatrix}, \tag{33}$$

and

$$\mathbf{h}_2(\mathbf{b}) = \begin{pmatrix} b_1 \\ 0 \\ b_2 \end{pmatrix} + \mathbf{o}_2 = \begin{pmatrix} b_1 + \pi \\ 0 \\ b_2 + \frac{3\pi}{2} \end{pmatrix}. \tag{34}$$

Take $[\mathbf{a}] = [-0.1, 0.1] \times [-0.1, 0.1]$.

Step 1. We have

$$[\mathbf{x}_a] = [\mathbf{h}_1]([\mathbf{a}]) = \begin{pmatrix} 0 \\ [-0.1, 0.1] \\ [-0.1 + \frac{\pi}{2}, 0.1 + \frac{\pi}{2}] \end{pmatrix}. \tag{35}$$

Step 2. We need to consider the variational equation:

$$\dot{\mathbf{J}} = \frac{\partial \mathbf{f}(\mathbf{x})}{\partial \mathbf{x}} \cdot \mathbf{J}, \tag{36}$$

i.e.,

$$\begin{pmatrix} \dot{J}_{11} & \dot{J}_{12} & \dot{J}_{13} \\ \dot{J}_{21} & \dot{J}_{22} & \dot{J}_{23} \\ \dot{J}_{31} & \dot{J}_{32} & \dot{J}_{33} \end{pmatrix} = \begin{pmatrix} 0 & 0 & 0 \\ 0 & 0 & \cos x_3 \\ 0 & 0 & 0 \end{pmatrix} \cdot \begin{pmatrix} J_{11} & J_{12} & J_{13} \\ J_{21} & J_{22} & J_{23} \\ J_{31} & J_{32} & J_{33} \end{pmatrix}. \tag{37}$$

Using an interval integration for both (31) and (37), for an initial vector $[\mathbf{x}_a]$ we get a tube for $[\mathbf{x}](t) = [\mathbf{\Phi}]([\mathbf{x}_a], t)$ and a tube for $[\mathbf{J}](t) = [\frac{\partial \mathbf{\Phi}}{\partial \mathbf{x}}]([\mathbf{x}_a], t)$.

Step 3. Since $g_2(\mathbf{x}) = x_2$, we get the Poincaré interval $[\tau_b]$ from the second component of $[\mathbf{x}](t)$. We get

$$\tau_b \in [\tau_b] = [2.82, 3.47]. \tag{38}$$

Step 4. From the tube $[\mathbf{x}](t)$, we extract $[\mathbf{x}_b] = [\mathbf{x}]([\tau_b])$. We get

$$[\mathbf{x}_b] = [2.82, 3.47] \times [-0.63, 0.63] \times [4.29, 5.14]. \tag{39}$$

Step 5,6. We get

$$[\mathbf{J}_q] = \begin{pmatrix} 1 & [1, 1.1] & [-2.41, -1.60] \\ [-0.01, 0.01] & [-0.1, 0.09] & [-0.64, 0.7] \\ [-0.01, 0.01] & [1, 1.1] & [-1.41, -0.69] \end{pmatrix}. \tag{40}$$

Step 7. We get

$$[\mathbf{b}] = \begin{pmatrix} 1 & 0 & 0 \\ 0 & 0 & 1 \end{pmatrix} \left([\mathbf{x}_b] - \begin{pmatrix} \pi \\ 0 \\ \frac{3\pi}{2} \end{pmatrix} \right). \tag{41}$$

Step 8. We get the degenerate matrix

$$[\mathbf{H}_2] = [\frac{\partial \mathbf{h}_2}{\partial \mathbf{x}}]([\mathbf{b}])) = \begin{pmatrix} 1 & 0 \\ 0 & 0 \\ 0 & 1 \end{pmatrix}. \tag{42}$$

Step 9. We get

$$[\mathbf{J_p}] = \begin{pmatrix} 1 & 0 & 0 \\ 0 & 0 & 1 \end{pmatrix} \cdot [\mathbf{J}_q] \cdot \begin{pmatrix} 0 & 0 \\ 1 & 0 \\ 0 & 1 \end{pmatrix} = \begin{pmatrix} [0.99, 1.1] & [-2.41, -1.60] \\ [0.99, 1.1], & [-1.41, -0.69] \end{pmatrix}. \tag{43}$$
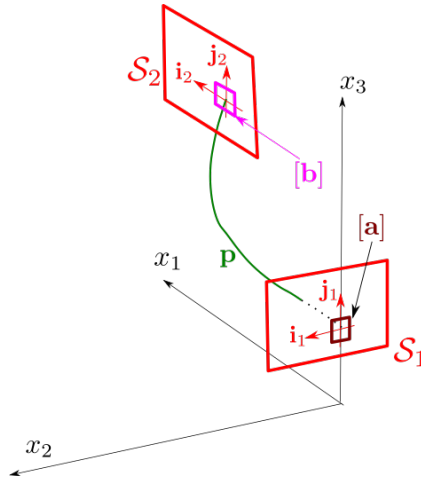

Figure 8: Example of Poincaré interval extension

3 Rolling navigation

3.1 Principle

We consider the robot moving on a plane described by the Dubins car model [32]

$$\begin{cases} \dot{x}_1 &= \cos x_3 \\ \dot{x}_2 &= \sin x_3 \\ \dot{x}_3 &= u, \end{cases} \tag{44}$$

where (x_1, x_2) is the position of the robot, x_3 is its heading and u is the input. The robot has no possibility to measure its state, neither its position nor its heading. It is only able to measure a function $\varphi(x_1, x_2)$ of its position such as a temperature or an altitude. We want that the robot moves along the

wanted curve $\varphi(x_1, x_2) = 0$. For this, we suggest to use the Trinity pattern proposed in [1] which yields a *rolling* behavior for the motion. The stability of the resulting navigation has been shown experimentally in [1] with an autonomous plane turning around a cloud with an unknown shape.

Now, to our knowledge, no theoretical analysis has been provided in the literature.

The principle of the rolling navigation is to alternate between a circle of radius ρ_0 when $\varphi < 0$ and a circle of radius ρ_1 when $\varphi > 0$, as illustrated by Figure 9. The left figure illustrates the ideal situation where the robot starts on the wanted curve $\varphi = 0$ (which is approximated by a line) with an incident angle of $\frac{\pi}{2}$. The robot follows the circle of radius ρ_0 until $\varphi = 0$, taking $u = \frac{1}{\rho_0}$. With a counter, the robot measures the elapsed time c_0. We should have $c_0 = \rho_0 \pi$. Then the robot follows the circle of radius ρ_1 for a time c_1 in order to be on the wanted line again. For k_1, k_2 in $\mathbb{N}$, we should have

$$k_1 \frac{c_1}{\rho_1} + k_2 \frac{c_0}{\rho_0} = (k_1 + k_2)\pi, \tag{45}$$

i.e.,

$$c_1 = \rho_1 \left(\pi + \frac{k_2}{k_1} \left(\pi - \frac{c_0}{\rho_0} \right) \right). \tag{46}$$

Take for instance $k_1 = 2$, $k_2 = 1$. We get

$$c_1 = \rho_1 \frac{3\pi - \frac{c_0}{\rho_0}}{2} = \rho_1 \pi. \tag{47}$$

If we have no uncertainties, the robot will be on the wanted line with an incidence angle of $\frac{\pi}{2}$.

3.2 Stability along the path

The question we need to study now, is the stability along the path $\varphi = 0$ for the chosen k_1, k_2. Consider the case where $\beta \neq \frac{\pi}{2}$ and assume that we are on the wanted line. The robot follows the circle of radius ρ_0 until $\varphi = 0$, taking $u = \frac{1}{\rho_0}$. It measures an elapsed time of $c_0 = \rho_0 \alpha_0$, where α_0 is the corresponding angle and then follows the circle of radius ρ_1 for a time c_1 given by (47). We understand that we are not anymore on the wanted line and proving the stability is not trivial.
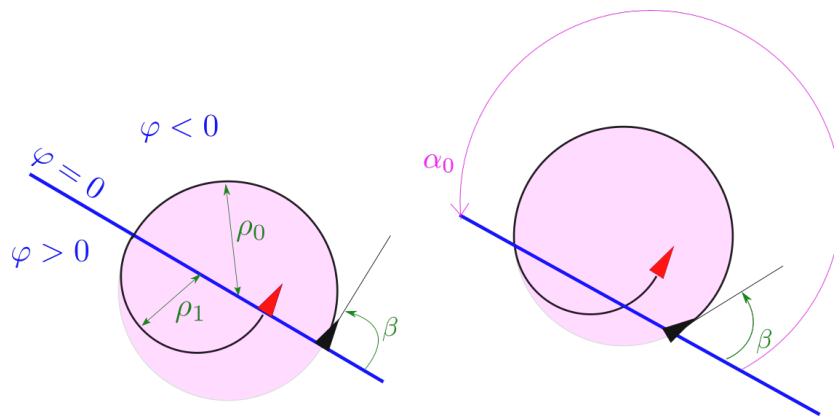
Figure 9: Left: The incidence angle $\beta = \frac{\pi}{2}$ is the right. Right: $\beta \neq \frac{\pi}{2}$ should be compensated

Take for simplicity $\rho_0 = 1, \rho_1 = \frac{1}{2}$.

Figure 10 shows a block diagram with the Dubins car and the controller. The controller has a single input corresponding to φ. It has two state variables: $q \in \{0,1\}$ and the counter $c \in [-\frac{\pi}{2}, \frac{\pi}{2}]$. It generates the control u.
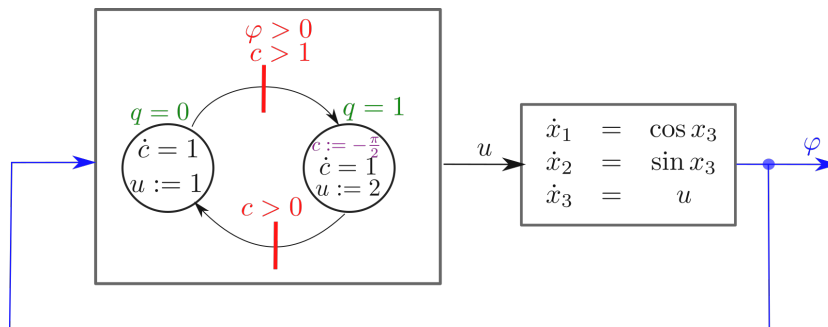

Figure 10: The controller is an automaton which controls our robot

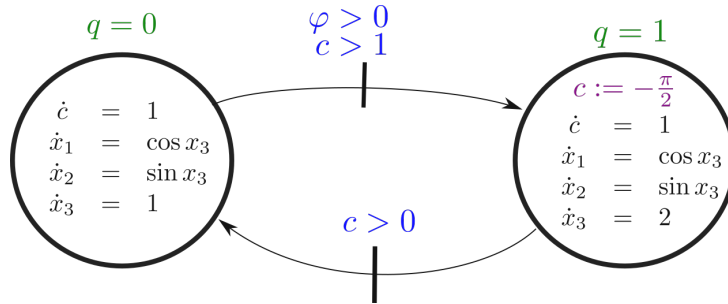The hybrid automaton representing our controlled system is given by Figure 11.

Figure 11: The corresponding trajectory is expected to roll on the curve $\varphi = 0$ in a stable way

3.3 Stability of a periodic orbit

Stability along a path can be simplified by a stability along a periodic orbit in the state space, by taking into account the symmetries by translation and by rotation of the problem. We consider a linear approximation of φ and we change the coordinate frame so that $\varphi > 0$ translates into $x_2 < 0$. This is illustrated by Figure 12.
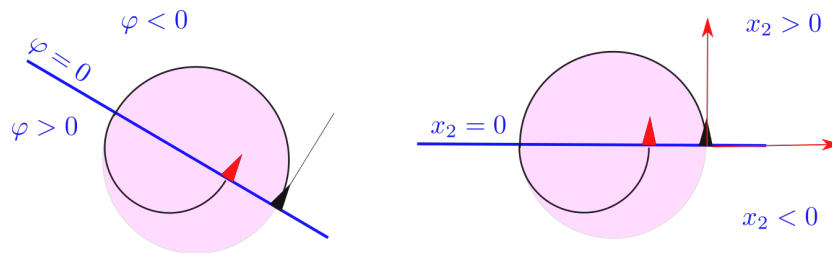

Figure 12: Left: The function φ is assumed to be linear. Right: simplification after a change of the coordinate frame

We want to prove the stability with respect to (q, c, x_2, x_3) at the point $(0, 0, 0, \frac{\pi}{2})$. The corresponding hybrid automaton is depicted in Figure 13. The state variable x_1 has been removed since its stability is not of interest.
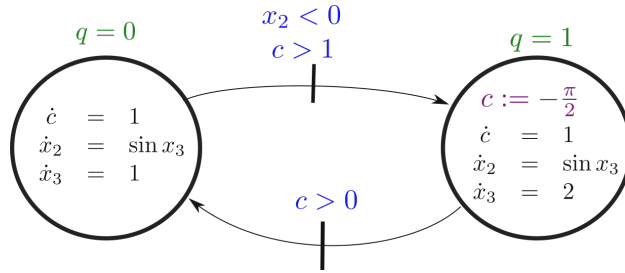
Figure 13: The periodic orbit generated by this automaton is stable if we start at $(q, c, x_2, x_3) = (0, 0, 0, \frac{\pi}{2})$

4 Proving the stability of rolling navigation

In this section, we propose to use analytical expressions of the Poincaré maps and their Jacobian to have a better understanding of how they are computed. Later, we will show that we do not need any analytical expression to prove the stability.

For the sake of clarity, we added an intermediate state $q = \frac{1}{2}$, as illustrated by Figure 14. This state, called the *jump,* is fleeting, *i.e.*, the state stays inside the jump state for 0 sec, or equivalently, as soon as it is inside $q = \frac{1}{2}$, it jumps to $q = 1$. In the jump, we added $x_3 := x_3 - 2\pi$ which is a non transformation, since x_3 is an angle. Now, this transformation allows us to have a bounded x_3 and to reason in the Cartesian line for x_3 instead of the trigonometric circle. Otherwise, the angle x_3 would increase by 2π at each lap of the hybrid automaton.
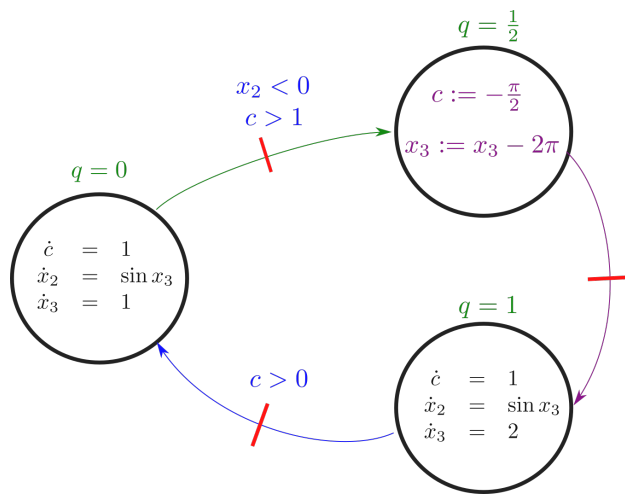
Figure 14: The trajectory generated by this automaton is stable at $(q, c, x_2, x_3) = (0, 0, 0, \frac{\pi}{2})$

4.1 Periodic orbit

If we simulate the system, starting from $(q, c, x_2, x_3) = (0, 0, 0, \frac{\pi}{2})$, we get the periodic orbit depicted in Figure 15 in the (c, x_2, x_3)-space. The red transitions of Figure 14 become the three red two-dimensional Poincaré sections of Figure 15. We switch from one surface to another using the partial Poincaré maps $\mathbf{p}_0, \mathbf{p}_{\frac{1}{2}}, \mathbf{p}_1$.
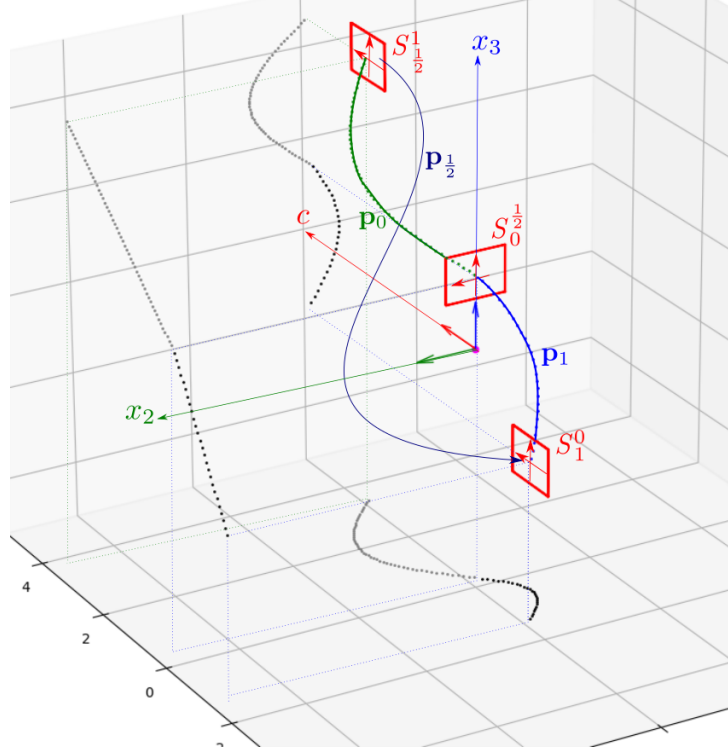
Figure 15: Periodic orbit in the (c, x_2, x_3)-space. The gray curves correspond to the three projections of the trajectory on each of the three canonical vertical planes

4.2 Equilibrium

Proposition. Assume that at time $t = 0$, we are at the state

$$(q, c, x_2, x_3) = (0, 0, 0, \frac{\pi}{2}). \tag{48}$$

Then at time $t = \frac{3\pi}{2}$, we will come back to the same state.

   Proof. Let us start at $t = 0$. We have

$$
\begin{aligned}
c(t) &= t \\
x_2(t) &= x_2(0) + \int_0^t \sin(x_3(\tau)) \cdot d\tau = \int_0^t \sin(\frac{\pi}{2} + \tau) \cdot d\tau \\
&= \int_0^t \cos(\tau) \cdot d\tau = \sin(t) \\
x_3(t) &= \frac{\pi}{2} + t.
\end{aligned} \tag{49}
$$

When $t = \pi$, we have $x_2(t) = 0$ and we switch to $q = \frac{1}{2}$. The state is now

$$(q, c, x_2, x_3) = (\frac{1}{2}, \pi, 0, \frac{3\pi}{2}). \tag{50}$$

We immediately jump to $(1, -\frac{\pi}{2}, 0, -\frac{\pi}{2})$.

As long as we stay with $q = 1$, we have

$$
\begin{aligned}
c(t) &= -\tfrac{\pi}{2} + (t - \pi) \\
x_2(t) &= x_2(\pi) + \int_\pi^t \sin(x_3(\tau)) \cdot d\tau \\
&= -\int_\pi^t \sin(\tfrac{\pi}{2} - 2\tau) \cdot d\tau = -\int_\pi^t \cos(2\tau) \cdot d\tau \\
&= -\left[\tfrac{1}{2}\sin(2\tau)\right]_\pi^t = -\tfrac{1}{2} \cdot \sin(2t) \\
x_3(t) &= x_3(\pi) + \int_\pi^t 2 \cdot d\tau = -\tfrac{\pi}{2} + 2(t - \pi) = 2t - \tfrac{5\pi}{2}.
\end{aligned}
\tag{51}
$$

When $t = \frac{3\pi}{2}$, we have $c(t) = 0$ and switch back to $q = 0$. The state it now

$$
\begin{aligned}
(q, c, x_2, x_3) &= (0, 0, -\tfrac{1}{2} \cdot \sin(2 \cdot \tfrac{3\pi}{2}), 2 \cdot \tfrac{3\pi}{2} - \tfrac{5\pi}{2}) \\
&= (0, 0, 0, \tfrac{\pi}{2}).
\end{aligned}
\tag{52}
$$

We thus came back to the initial state.

4.3 Expression for $\mathbf{p}_0$

Take $t = 0$, and assume that we are at the state

$$
(q, c, x_2, x_3) = (0, 0, \tilde{x}_2, \frac{\pi}{2} + \tilde{x}_3).
\tag{53}
$$

It means that we are on the Poincaré surface $\mathcal{S}_0^{\frac{1}{2}}$, at the coordinates $\tilde{x}_2, \tilde{x}_3$.

As long as we satisfy $q = 0$, we have

$$
\begin{aligned}
c(t) &= t \\
x_2(t) &= \tilde{x}_2 + \int_0^t \sin(x_3(\tau)) \cdot d\tau = \tilde{x}_2 + \int_0^t \sin(\tfrac{\pi}{2} + \tau + \tilde{x}_3) \cdot d\tau \\
&= \tilde{x}_2 + \int_0^t \cos(\tau + \tilde{x}_3) \cdot d\tau = \tilde{x}_2 + [\sin(\tau + \tilde{x}_3)]_0^t \\
&= \tilde{x}_2 + \sin(t + \tilde{x}_3) - \sin(\tilde{x}_3) \\
x_3(t) &= \tfrac{\pi}{2} + \tilde{x}_3 + t.
\end{aligned}
\tag{54}
$$

We define

$$
\begin{aligned}
t_1(\tilde{x}_2, \tilde{x}_3) &= \min\{t > 0 \mid \tilde{x}_2 + \sin(t + \tilde{x}_3) - \sin(\tilde{x}_3) = 0\} \\
&= \min\{t > 0 \mid \sin(t + \tilde{x}_3) = \sin(\tilde{x}_3) - \tilde{x}_2\} \\
&= \pi - \arcsin(\sin(\tilde{x}_3) - \tilde{x}_2) - \tilde{x}_3.
\end{aligned}
\tag{55}
$$

We thus get the first partial Poincaré map

$$
\begin{aligned}
\mathbf{p}_0 \begin{pmatrix} \tilde{x}_2 \\ \tilde{x}_3 \end{pmatrix} &= \begin{pmatrix} t_1(\tilde{x}_2, \tilde{x}_3) \\ \tfrac{\pi}{2} + \tilde{x}_3 + t_1(\tilde{x}_2, \tilde{x}_3) \end{pmatrix} - \begin{pmatrix} \pi \\ \tfrac{3\pi}{2} \end{pmatrix} \\
&= \begin{pmatrix} -\arcsin(\sin(\tilde{x}_3) - \tilde{x}_2) - \tilde{x}_3 \\ -\arcsin(\sin(\tilde{x}_3) - \tilde{x}_2) \end{pmatrix}.
\end{aligned}
\tag{56}
$$

A first order approximation of this function is

$$
\mathbf{p}_0 \begin{pmatrix} dx_2 \\ dx_3 \end{pmatrix} = \begin{pmatrix} -\arcsin(\sin(dx_3) - dx_2) - dx_3 \\ -\arcsin(\sin(dx_3) - dx_2) \end{pmatrix}
$$
$$
= \begin{pmatrix} -2dx_3 + dx_2 \\ -dx_3 + dx_2 \end{pmatrix}
$$
$$
= \underbrace{\begin{pmatrix} 1 & -2 \\ 1 & -1 \end{pmatrix}}_{=\mathbf{J}_0} \begin{pmatrix} dx_2 \\ dx_3 \end{pmatrix}. \tag{57}
$$

These results are consistent with those obtained in Section 2.8.

4.4   Expression for $\mathbf{p}_{\frac{1}{2}}$

The jump is the affine map defined by

$$
\mathbf{p}_{\frac{1}{2}} \begin{pmatrix} \tilde{c} \\ \tilde{x}_3 \end{pmatrix} = \begin{pmatrix} 0 & 0 \\ 0 & 1 \end{pmatrix} \begin{pmatrix} \tilde{c} \\ \tilde{x}_3 \end{pmatrix} = \begin{pmatrix} 0 \\ \tilde{x}_3 \end{pmatrix}. \tag{58}
$$

Thus, we get

$$
\mathbf{p}_{\frac{1}{2}} \circ \mathbf{p}_0 \begin{pmatrix} [-0.1, 0.1] \\ [-0.1, 0.1] \end{pmatrix} \subset \begin{pmatrix} 0 \\ [-0.43, 0.43] \end{pmatrix} \tag{59}
$$

and

$$
\mathbf{J}_{\mathbf{p}_{\frac{1}{2}}} = \begin{pmatrix} 0 & 0 \\ 0 & 1 \end{pmatrix}. \tag{60}
$$

4.5   Expression for $\mathbf{p}_1$

Take $t = 0$, and assume that we are at the state

$$
(q, c, x_2, x_3) = (1, -\frac{\pi}{2} + \tilde{c}, 0, -\frac{\pi}{2} + \tilde{x}_3). \tag{61}
$$

As long as we satisfy $q = 1$, we have

$$
\begin{aligned}
c(t) &= -\frac{\pi}{2} + \tilde{c} + t \\
x_2(t) &= 0 + \int_0^t \sin(x_3(\tau)) \cdot d\tau = \int_0^t -\sin(\frac{\pi}{2} - 2\tau - \tilde{x}_3) \cdot d\tau \\
&= -\int_0^t \cos(2\tau + \tilde{x}_3) \cdot d\tau \\
&= -\left[\frac{1}{2} \sin(2\tau + \tilde{x}_3)\right]_0^t = \frac{1}{2} \sin(\tilde{x}_3) - \frac{1}{2} \sin(2t + \tilde{x}_3) \\
x_3(t) &= -\frac{\pi}{2} + \tilde{x}_3 + 2t.
\end{aligned} \tag{62}
$$

We define

$$
t_2(\tilde{c}, \tilde{x}_3) = \min \left\{ t > 0 \mid -\frac{\pi}{2} + \tilde{c} + t = 0 \right\} = \frac{\pi}{2} - \tilde{c}. \tag{63}
$$

We have

$$
\begin{aligned}
\mathbf{p}_1 \begin{pmatrix} \tilde{c} \\ \tilde{x}_3 \end{pmatrix}
&= \begin{pmatrix} \frac{1}{2}\sin(\tilde{x}_3) - \frac{1}{2}\sin(2t_2(\tilde{c},\tilde{x}_3)+\tilde{x}_3) \\ -\frac{\pi}{2}+\tilde{x}_3+2t_2(\tilde{c},\tilde{x}_3) \end{pmatrix} - \begin{pmatrix} 0 \\ \frac{\pi}{2} \end{pmatrix} \\
&= \begin{pmatrix} \frac{1}{2}\sin(\tilde{x}_3) - \frac{1}{2}\sin\left(2\left(\frac{\pi}{2}-\tilde{c}\right)+\tilde{x}_3\right) \\ -\frac{\pi}{2}+\tilde{x}_3+2\left(\frac{\pi}{2}-\tilde{c}\right)-\frac{\pi}{2} \end{pmatrix} \\
&= \begin{pmatrix} \frac{1}{2}\sin(\tilde{x}_3) - \frac{1}{2}\sin(\pi-2\tilde{c}+\tilde{x}_3) \\ \tilde{x}_3-2\tilde{c} \end{pmatrix} \\
&= \begin{pmatrix} \frac{1}{2}\sin(\tilde{x}_3) - \frac{1}{2}\sin(2\tilde{c}-\tilde{x}_3) \\ \tilde{x}_3-2\tilde{c} \end{pmatrix}.
\end{aligned}
\tag{64}
$$

A first order approximation of $\mathbf{p}_1$ is

$$
\begin{aligned}
\mathbf{p}_1 \begin{pmatrix} dc \\ dx_3 \end{pmatrix}
&= \begin{pmatrix} \frac{1}{2}\sin(dx_3) - \frac{1}{2}\sin(2dc-dx_3) \\ dx_3-2dc \end{pmatrix} \\
&= \begin{pmatrix} -dc+dx_3 \\ dx_3-2dc \end{pmatrix} \\
&= \underbrace{\begin{pmatrix} -1 & 1 \\ -2 & 1 \end{pmatrix}}_{=\mathbf{J}_1} \begin{pmatrix} dc \\ dx_3 \end{pmatrix}.
\end{aligned}
\tag{65}
$$

4.6   Poincaré map

We define

$$
\mathbf{p}\begin{pmatrix} \tilde{x}_2 \\ \tilde{x}_3 \end{pmatrix} = \mathbf{p}_1 \circ \mathbf{p}_{\frac{1}{2}} \circ \mathbf{p}_0 \begin{pmatrix} \tilde{x}_2 \\ \tilde{x}_3 \end{pmatrix}.
\tag{66}
$$

Since

$$
\mathbf{p}_0 \begin{pmatrix} \tilde{x}_2 \\ \tilde{x}_3 \end{pmatrix} \mapsto \begin{pmatrix} -\arcsin(\sin(\tilde{x}_3)-\tilde{x}_2)-\tilde{x}_3 \\ -\arcsin(\sin(\tilde{x}_3)-\tilde{x}_2) \end{pmatrix}
\tag{67}
$$

$$
\mathbf{p}_{\frac{1}{2}} \begin{pmatrix} \tilde{c} \\ \tilde{x}_3 \end{pmatrix} = \begin{pmatrix} 0 & 0 \\ 0 & 1 \end{pmatrix} \begin{pmatrix} \tilde{c} \\ \tilde{x}_3 \end{pmatrix} = \begin{pmatrix} 0 \\ \tilde{x}_3 \end{pmatrix}
\tag{68}
$$

$$
\mathbf{p}_1 \begin{pmatrix} \tilde{c} \\ \tilde{x}_3 \end{pmatrix} = \begin{pmatrix} \frac{1}{2}\sin(\tilde{x}_3) - \frac{1}{2}\sin(2\tilde{c}-\tilde{x}_3) \\ \tilde{x}_3-2\tilde{c} \end{pmatrix},
\tag{69}
$$

we get

$$
\mathbf{p}\begin{pmatrix} \tilde{x}_2 \\ \tilde{x}_3 \end{pmatrix} = \begin{pmatrix} \tilde{x}_2-\sin(\tilde{x}_3) \\ \arcsin(\tilde{x}_2-\sin(\tilde{x}_3)) \end{pmatrix}.
\tag{70}
$$

The Jacobian of $\mathbf{p}$ at $\mathbf{0}$ is

$$
\mathbf{J}_{\mathbf{p}}(\mathbf{0}) = \mathbf{J}_1 \cdot \mathbf{J}_{\frac{1}{2}} \cdot \mathbf{J}_0 = \begin{pmatrix} -1 & 1 \\ -2 & 1 \end{pmatrix}\begin{pmatrix} 0 & 0 \\ 0 & 1 \end{pmatrix}\begin{pmatrix} 1 & -2 \\ 1 & -1 \end{pmatrix} = \begin{pmatrix} 1 & -1 \\ 1 & -1 \end{pmatrix}, \tag{71}
$$

which is stable (all roots are in the unit disk). As a consequence, the periodic orbit is stable.

5   Basin of attraction

In this section, we want to find a subset of the state space of all states which will converge to the periodic orbit. It is sufficient to limit our analysis to a Poincaré section, say S_0^1. More precisely, we will find a centered box $\mathbb{X}_0$ inside S_0^1 such that $\mathbf{p}(\mathbb{X}_0) \subset \mathbb{X}_0$ in this case, $\mathbb{X}_0$ is positive invariant. Unfortunately, in our situation (which is not atypical), such a box does not exist and we can only find $k > 1$ such that $\mathbf{p}^k(\mathbb{X}_0) \subset \mathbb{X}_0$. This corresponds to the *periodic invariance* studied by Lee and Kouvaritakis in [33].

5.1   Find a periodic positive invariant box

To check the stability we take a small box containing 0, for instance

$$\mathbb{X}_0 = [-0.1, 0.1] \times [-0.1, 0.1],$$

which corresponds to the red box in Figure 16. If we compute the smallest box which contains $\mathbb{X}_0$ we find the blue box, which means that $\mathbf{p}(\mathbb{X}_0) \not\subset \mathbb{X}_0$. Now, we also get $\mathbf{p}^2(\mathbb{X}_0) \subset \mathbb{X}_0$ and $\mathbf{p}^3(\mathbb{X}_0) \subset \mathbb{X}_0$. We conclude that $\mathbb{X}_0$ is periodic positive invariant.

5.2   Find an asymptotically stable box

We now want to show that all initial state inside $\mathbb{X}_0$ will converge to 0. We use the centered form [2] for stability [23, 10]. For this, we follow the procedure given by relation (7). For $k = 1$, we do not get the enclosure. For $k = 2$, we get (see Equation (9)):

$$\left([\mathbf{J_p}] \left([\mathbf{p}] \left(\begin{array}{c} [\tilde{x}_2] \\ [\tilde{x}_3] \end{array} \right) \right) \right) \cdot \left([\mathbf{J_p}] \left(\begin{array}{c} [\tilde{x}_2] \\ [\tilde{x}_3] \end{array} \right) \right) \cdot \left(\begin{array}{c} [\tilde{x}_2] \\ [\tilde{x}_3] \end{array} \right) \subset \left(\begin{array}{c} [\tilde{x}_2] \\ [\tilde{x}_3] \end{array} \right). \quad (72)$$

For the Poincaré map and its Jacobian, we took:

$$\mathbf{p} \left(\begin{array}{c} \tilde{x}_2 \\ \tilde{x}_3 \end{array} \right) = \left(\begin{array}{c} \tilde{x}_2 - \sin(\tilde{x}_3) \\ \arcsin(\tilde{x}_2 - \sin(\tilde{x}_3)) \end{array} \right) \quad (73)$$

and

$$\mathbf{J_p} \left(\begin{array}{c} \tilde{x}_2 \\ \tilde{x}_3 \end{array} \right) = \left(\begin{array}{cc} 1 & -\cos(\tilde{x}_3) \\ \frac{1}{\sqrt{1-(\tilde{x}_2-\sin(\tilde{x}_3))^2}} & \frac{-\cos(\tilde{x}_3)}{\sqrt{1-(\tilde{x}_2-\sin(\tilde{x}_3))^2}} \end{array} \right). \quad (74)$$

Following [23] we get that all trajectories initialized in $\mathbb{X}_0$ will converge to $\mathbf{0}$ and will stay inside $\mathbf{p}(\mathbb{X}_0)$. We can write this property under the form $\mathbf{p}^\infty(\mathbb{X}_0) = \mathbf{0}$.

5.3 Find an asymptotically stable box using an interval integration

In the general case, we do not have any analytical expression for the flow. The procedure has to be applied using an interval integration. We give here all intermediate results related to our test-case (see [34] for more details). We start from

$$[\mathbf{a}] = [-0.01, 0.01]. \tag{75}$$

First lap. We get

$$[\tau_b] = [3.1114, 3.17179], \tag{76}$$

$$[\mathbf{x}_b] = \begin{pmatrix} [3.1114, 3.17179] \\ [-0.0603952, 0.0603829] \\ [4.67219, 4.75259] \end{pmatrix}. \tag{77}$$

The monodromy matrix for $\mathbf{p}_0$ is

$$[\mathbf{J}]([\tau_b]) = \begin{pmatrix} [1, 1] & [-10^{-10}, 10^{-10}] & [-10^{-10}, 10^{-10}] \\ [-10^{-10}, 10^{-10}] & [1, 1] & [-2.01996, -1.97913] \\ [-10^{-10}, 10^{-10}] & [-10^{-10}, 10^{-10}] & [1, 1] \end{pmatrix} \tag{78}$$

and the Jacobian matrix for $\mathbf{p}_0$ is

$$[\mathbf{J}_{\mathbf{p}_0}] = \begin{pmatrix} [1, 1.00081] & [-2.02159, -1.97913] \\ [1, 1.00081] & [-1.02159, -0.979133] \end{pmatrix}. \tag{79}$$

We have the jump and then, we switch to $\mathbf{p}_1$. We get

$$[\tau_b] = [1.5708, 1.5709] \tag{80}$$

and

$$[\mathbf{x}_b] = \begin{pmatrix} [-10^{-10}, 10^{-10}] \\ [-0.0417802, 0.0417865] \\ [1.5306, 1.611] \end{pmatrix}. \tag{81}$$

For the monodromy matrix, we get

$$[\mathbf{J}]([\tau_b]) = \begin{pmatrix} [1, 1] & [-10^{-10}, 10^{-10}] & [-10^{-10}, 10^{-10}] \\ [-10^{-10}, 10^{-10}] & [1, 1] & [0.958986, 1.03941] \\ [-10^{-10}, 10^{-10}] & [-10^{-10}, 10^{-10}] & [1, 1] \end{pmatrix}. \tag{82}$$

The Jacodian matrix is

$$[\mathbf{J}_{\mathbf{p}_1}] = \begin{pmatrix} [1, 1.00081] & [-2.02159, -1.97913] \\ [1, 1.00081] & [-1.02159, -0.979133] \end{pmatrix}, \tag{83}$$

and the interval enclosure of the Poincaré map becomes

$$[\mathbf{p}]\,([\mathbf{a}]) = \begin{pmatrix} [-0.021021, 0.021021] \\ [-0.020224, 0.020224] \end{pmatrix}. \tag{84}$$

Second lap. We perform the same type of computation as for the first lap and we get

$$[\mathbf{p} \circ \mathbf{p}]\,([\mathbf{a}]) = \begin{pmatrix} [-0.00512577, 0.00512577] \\ [-0.00178467, 0.00178467] \end{pmatrix}. \tag{85}$$

For all other details, see [34].

From these results, we have easily checked that $[\mathbf{J_p}]([\mathbf{p}][\mathbf{a}]) \cdot [\mathbf{J_p}]([\mathbf{a}]) \cdot [\mathbf{a}] \subset [\mathbf{a}]$ and we conclude the asymptotic stability.

5.4 Capture basin

We now want to characterize a set larger than $\mathbb{X}_0 = [-0.1, 0.1] \times [-0.1, 0.1]$ for $(\tilde{x}_2, \tilde{x}_3)$ which will converge to $\mathbf{0}$. Such a set is called a *capture basin* [16]. We know from [35, 36] that, since $\mathbb{X}_0$ is a capture basin, $\mathbf{p}^{-k}(\mathbb{X}_0)$, $k \geq 0$ is also a basin. Indeed all points $(\tilde{x}_2, \tilde{x}_3) \in \mathbf{p}^{-k}(\mathbb{X}_0)$ will be such that $\mathbf{p}^k(\tilde{x}_2, \tilde{x}_3) \in \mathbb{X}_0$ and will thus converge to $\mathbf{0}$.

The orange strip in Figure (16) corresponds $\mathbb{X}_1 = \mathbf{p}^{-1}(\mathbb{X}_0)$ and extends from $-\frac{\pi}{2}$ to $\frac{\pi}{2}$, The green set corresponds to $\mathbb{X}_2 = \mathbf{p}^{-2}(\mathbb{X}_0)$.
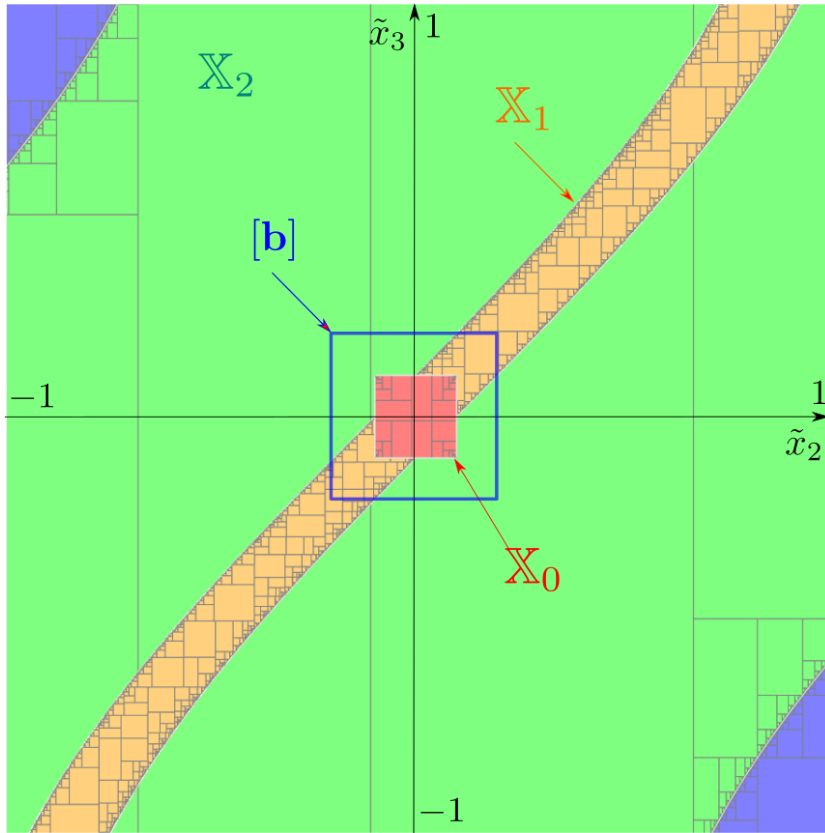
Figure 16: Each point in $\mathbb{X}_2$ (green) will first enter in the orange set $\mathbb{X}_1$, then in the red set $\mathbb{X}_0$. Once in $\mathbb{X}_0$, it will converge to $\mathbf{0}$

All the properties we have proven can be summarized by Figure 17. From this graph, we read that $\mathbf{p}^k(\mathbb{X}_2) \subset \mathbb{X}_0$ for $k \in \{2, 4, 5, 6, \dots\}$. But, we have $\mathbf{p}^3(\mathbb{X}_2) \subset [\mathbf{b}]$ which may be outside $\mathbb{X}_0$. Moreover, we have $\mathbf{p}^\infty(\mathbb{X}_2) = \mathbf{0}$. The non inclusion monotonicity of the chain is due to the fact that $\mathbb{X}_0$ is not positive invariant. It is only *periodic* positive invariant.
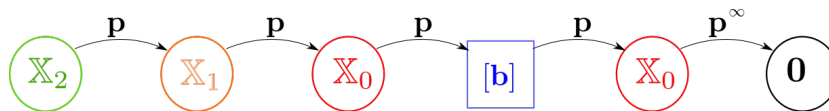

Figure 17: Each point in $\mathbb{X}_2$ (green) will converge to $\mathbf{0}$ and will cross a non-nested chain of sets

5.5 Illustration

The stability property has been proven for a linear $\varphi(x_1, x_2)$. In order to illustrate the behavior of our controller for an arbitrary φ, we consider that φ corresponds to the Hippopede of Proclus given by

$$\varphi(x_1, x_2) = 9x_1^2 + x_2^2 - \left(x_1^2 + y_2^2\right)^2. \tag{86}$$

Of course, this equation is not known by our controller which is based on the fact that $\varphi(x_1, x_2)$ is linear. We take for the initial state vector of the robot $\mathbf{x} = (3, 0, 1)$ and for the controller $q = 0$, $c = 0$. The simulation of the controlled robot generates Figure 18 and shows that without any compass, measuring only the sign of a scalar unknown function φ depending of the position, we are able to move along the curve $\varphi(x_1, x_2) = 0$ in a stable and robust way.
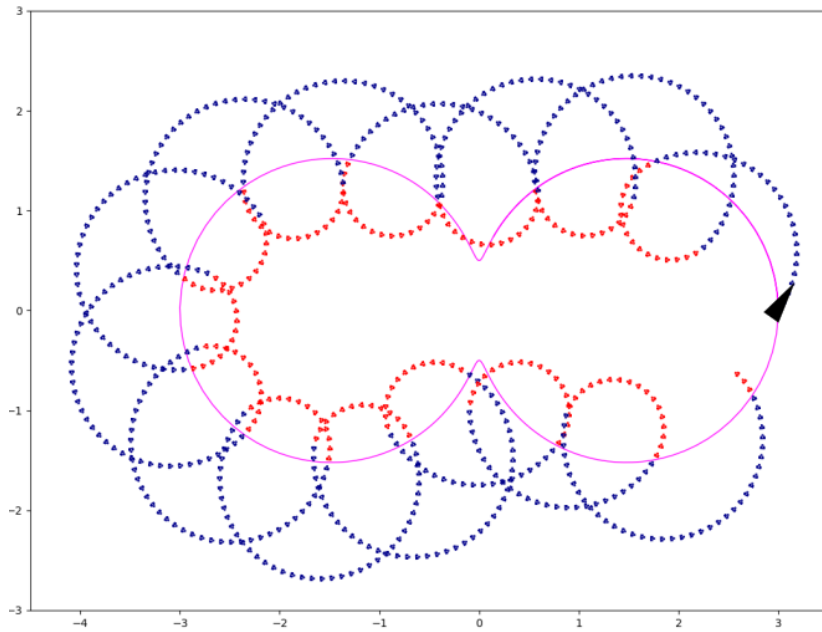

Figure 18: The robot rolls along the Hippopede. The frame box is $[-4.5, 3.5] \times [-3, 3]$.

6 Conclusion

In this paper, we have proposed an interval extension of Poincaré maps to show the stability of hybrid dynamical systems with respect to a periodic

orbit. The approach has been illustrated on the rolling navigation. This type of navigation can be used in an unstructured environment, where few sensors can be used by the robot. Then, we extended our approach to characterize an inner approximation of the attraction domain of the periodic orbit.

The mathematical tools used here were well known [9] for studying attractors of continuous dynamical systems. Our main contribution is the adaptation of these tools, mainly based on the rigorous computation of Poincaré maps, to prove the stability of periodic orbits of hybrid systems. One limitation of the approach is that we have to perform an undefined number of laps before proving the periodic stability. An extension would be the use of ellipsoids instead of boxes. This would allow us to perform only one lap by choosing the right shape for the ellipsoid. Moreover, each time we intersect a surface, the wrapping effect introduced by the intersection would significantly decrease with ellipsoids, since the intersection between one ellipsoid and one plane is still an ellipsoid.

The Python programs associated to all examples can be found here: https://www.ensta-bretagne.fr/jaulin/rolling.html

References

[1] T. Verdu, N. Maury, P. Narvor, F. Seguin, G. Roberts, F. Couvreux, G. Cayez, M. Bronz, G. Hattenberger, and S. Lacroix. Experimental flights of adaptive patterns for cloud exploration with uavs. In *IEEE/RSJ International Conference on Intelligent Robots and Systems, IROS 2020, Las Vegas, NV, USA, October 24, 2020 - January 24, 2021*, pages 1429–1435. IEEE, 2020.

[2] R. E. Moore. *Methods and Applications of Interval Analysis*. SIAM, Philadelphia, PA, 1979.

[3] R. B. Kearfott and V. Kreinovich, editors. *Applications of Interval Computations*. Kluwer, Dordrecht, the Netherlands, 1996.

[4] S. Rohou. *Reliable robot localization: a constraint programming approach over dynamical systems*. PhD dissertation, Université de Bretagne Occidentale, ENSTA-Bretagne, France, December 2017.

[5] S. Rohou, L. Jaulin, L. Mihaylova, F. Le Bars, and S. Veres. *Reliable robot localization; A Constraint-Programming Approach Over Dynamical Systems*. ISTE, WILEY, 2019.

[6] V. Drevelle and P. Bonnifait. Localization confidence domains via set inversion on short-term trajectory. *IEEE Transactions on Robotics*, 2013.

[7] W. Tucker. The Lorenz Attractor Exists. *Comptes Rendus de l'Académie des Sciences*, 328(12):1197–1202, 1999.

[8] D. Wilczak and P. Zgliczynski. Cr-Lohner algorithm. *Schedae Informaticae*, 20:9–46, 2011.

[9] Tomasz Kapela, Marian Mrozek, Daniel Wilczak, and Piotr Zgliczynski. CAPD: : Dynsys: A flexible C++ toolbox for rigorous numerical analysis of dynamical systems. *Commun. Nonlinear Sci. Numer. Simul.*, 101:105578, 2021.

[10] A. Rauh, A. Bourgois, and L. Jaulin. Verifying provable stability domains for discrete-time systems using ellipsoidal state enclosures. *Acta Cybernetica, submitted*, 2021.

[11] A. Bourgois. *Safe and Collaborative Autonomous Underwater Docking.* PhD dissertation, Université de Bretagne occidentale, Brest, France, 2021.

[12] T. Le Mézo, L. Jaulin, and B. Zerr. An interval approach to compute invariant sets. *IEEE Transaction on Automatic Control*, 62:4236–4243, 2017.

[13] N. Ramdani and N. Nedialkov. Computing Reachable Sets for Uncertain Nonlinear Hybrid Systems using Interval Constraint Propagation Techniques. *Nonlinear Analysis: Hybrid Systems*, 5(2):149–162, 2011.

[14] Nacim Ramdani, Louise Travé-Massuyès, and Carine Jauberthie. Mode discernibility and bounded-error state estimation for nonlinear hybrid systems. *Autom.*, 91:118–125, 2018.

[15] A. Bourgois, A. Chaabouni, A. Rauh, and L. Jaulin. Proving the stability of navigation cycles. In *SCAN*, 2021.

[16] J.-P. Aubin. Viability Kernels and Capture Basins of Sets Under Differential Inclusions. *SIAM Journal on Control and Optimization*, 40(3):853–881, January 2001.

[17] M. Lhommeau, L. Jaulin, and L. Hardouin. Capture Basin Approximation using Interval Analysis. *International Journal of Adaptative Control and Signal Processing*, 25(3):264–272, 2011.

[18] S. Ratschan and Z. She. Providing a Basin of Attraction to a Target Region of Polynomial Systems by Computation of Lyapunov-like Functions. *SIAM J. Control and Optimization*, 48(7):4377–4394, 2010.

[19] A. Goldsztejn and G. Chabert. Estimating the robust domain of attraction for non-smooth systems using an interval lyapunov equation. *Automatica*, 100:371–377, 2019.

[20] O. Hachicho and B. Tibken. Estimating domains of Attraction of a Class of Nonlinear Dynamical Systems with LMI Methods Based on the Theory of Moments. In *Proceedings of the 41st IEEE Conference on Decision and Control, 2002.*, volume 3, pages 3150–3155, 2002.

[21] T. Pursche, R. Swiatlak, and B. Tibken. Estimation of the Domain of Attraction for Nonlinear Autonomous Systems Using a Bezoutian Approach. In *2016 SICE International Symposium on Control Systems (ISCS)*, pages 1–6, 2016.

[22] R. Swiatlak, B. Tibken, T. Paradowski, and R. Dehnert. Determination of the Optimal Quadratic Lyapunov Function for Nonlinear Autonomous Systems via Interval Arithmetic. In *2015 European Control Conference (ECC)*, pages 297–303, 2015.

[23] A. Bourgois and L. Jaulin. Interval centred form for proving stability of non-linear discrete-time system. In *SNR, Vienna*, 2020.

[24] A. Rauh, A. Bourgois, L. Jaulin, and J. Kersten. Ellipsoidal enclosure techniques for a verified simulation of initial value problems for ordinary differential equations. In *ICCAD 2021, Grenoble, France*, 2021.

[25] J Lunze and F Lamnabhi-Lagarrigue. *Handbook of hybrid systems control: theory, tools, applications*. Cambridge University Press, England, 2009.

[26] A. Girard. Computation and stability analysis of limit cycles in piecewise linear hybrid systems. In *1st IFAC Conference on Analysis and Design of Hybrid Systems*, pages 181–186, 2003.

[27] V.I. Arnold. *Geometrical Methods In The Theory Of Ordinary Differential Equations*. Springer-Verlag, 1988.

[28] A. Rauh. *Sensitivity Methods for Analysis and Design of Dynamic Systems with Applications in Control Engineering*. Shaker–Verlag, 2017.

[29] R. Lohner. Enclosing the solutions of ordinary initial and boundary value problems. In E. Kaucher, U. Kulisch, and Ch. Ullrich, editors, *Computer Arithmetic: Scientific Computation and Programming Languages*, pages 255–286. BG Teubner, Stuttgart, Germany, 1987.

[30] Piotr Zgliczynski. C^1 lohner algorithm. *Found. Comput. Math.*, 2(4):429–465, 2002.

[31] Tomasz Kapela, Daniel Wilczak, and Piotr Zgliczynski. Recent advances in a rigorous computation of poincaré maps. *Commun. Nonlinear Sci. Numer. Simul.*, 110:106366, 2022.

[32] L. E. Dubins. On curves of minimal length with a constraint on average curvature, and with prescribed initial and terminal positions and tangents. *American Journal of Mathematics*, 79(3):497–516, 1957.

[33] Young Il Lee and Basil Kouvaritakis. Constrained robust model predictive control based on periodic invariance. *Autom.*, 42(12):2175–2181, 2006.

[34] A.Bourgois, A. Chaabouni, A. Rauh, and L. Jaulin. *Codes for stability of the rolling experiment, available at* https://www.ensta-bretagne.fr/jaulin/rolling.html. Robex, Lab-STICC, ENSTA-Bretagne, 2022.

[35] F. Blanchini and S. Miani. *Set-Theoretic Methods in Control*. Springer Science & Business Media, October 2007.

[36] J.-P. Aubin. *Viability Theory*. Springer Science and Business Media, may 2009.